aerospace

MDPI

Article

Expanding Known Performance Capabilities of Geared Turbofan Engine When Powered by LNG and Methanol

Sergios Villette *, Alexios Alexiou, Nikolaos Aretakis and Konstantinos Mathioudakis

Laboratory of Thermal Turbomachines, School of Mechanical Engineering, National Technical University of Athens, 15780 Athens, Greece; alexioua@mail.ntua.gr (A.A.); naret@mail.ntua.gr (N.A.); kmathiou@mail.ntua.gr (K.M.)

* Correspondence: ser_villet@mail.ntua.gr

Abstract: As aviation demand rises, fossil jet fuel consumption follows, thus increasing focus on sustainable aviation fuels to reduce aircraft greenhouse gas emissions. While advanced technologies and optimized operations play a role, alternative fuels, especially non-drop-in options like Liquefied Natural Gas (LNG) and methanol, offer promising potential for significant emission reductions if used in current aero-engines. LNG, a candidate near-term replacement of fossil jet fuel and methanol, even though a less conventional option in aviation, present advantages. Both fuels showcase the ability to generate the same thrust output by also achieving lower post-combustion temperatures, thereby enhancing component life and reducing emissions. Inversely, requesting equal post-combustion temperature as the baseline kerosene operation of the engine can produce greater thrust output, a much needed result for such fuels with low volumetric energy density, which causes greater take-off thrust demand mainly due to their larger tank requirements. This study uses advanced 0-D engine models coupled with detailed chemistry 1-D burner models and mission analysis tools to assess the aforementioned trends of LNG and methanol used to power a current geared turbofan engine. The aim of this work is to provide insights into the advantages, the limitations and the overall viability of the fuels in question as less polluting aviation fuels, addressing both environmental impact and operational feasibility in future aviation applications. According to findings of this article, when compared with Jet-A, LNG can reduce post-combustion temperature by an average of 1% or increase net-thrust by 3% while lowering CO_2, NO_x and CO emissions by 20%, 46% and 39%, respectively. Adversely, methanol is capable of lessening post-combustion temperature by 3% or enhancing thrust output by 10% while also reducing CO_2, NO_x and CO emissions by an average of 6%, 60% and 38%, respectively.

Keywords: aero-engine model; geared turbofan; methanol; LNG; chemical reactor network; PROOSIS

Academic Editor: Pedro Miguel Rebelo Resende

Received: 20 December 2024
Revised: 20 January 2025
Accepted: 24 January 2025
Published: 28 January 2025

Citation: Villette, S.; Alexiou, A.; Aretakis, N.; Mathioudakis, K. Expanding Known Performance Capabilities of Geared Turbofan Engine When Powered by LNG and Methanol. *Aerospace* **2025**, *12*, 96. https://doi.org/10.3390/aerospace12020096

1. Introduction

The aviation sector contributes to greenhouse gas (GHG) emissions, producing 2–3% of global carbon dioxide (CO_2) [1] and 2–5% of total anthropogenic GHGs [2–4], including CO_2, nitrous oxides and methane (CH_4) [5,6]. These emissions are apparently linked with global warming through radiative forcing, aviation-induced cloudiness, such as contrails, etc. [1,7,8]. While aviation's global impact is relatively small, its regional effects on air pollution can rival those of ground transportation, affecting public health [9,10].

Aviation's heavy reliance on fossil fuels challenges the sector's sustainability. Rising demand, geopolitical conflicts, such as the 2022 Ukraine War, and supply shortages

have driven up fuel prices, creating an energy crisis [11]. Despite modern aircraft being 75–80% more fuel-efficient than those of 50 years ago [3,12], projected air traffic growth of 4.3% annually over the next 20 years [13] will lead to increased fuel consumption and a corresponding 4% rise in emissions [4].

There is thus need to explore new, alternative fuels. International agreements, like the Paris Agreement, and industrial strategies, such as the European Green Deal, aim to achieve carbon neutrality by 2050, requiring annual CO_2 emission reductions of 4–8% [12,14]. These initiatives call for significant investments in alternative aviation fuels, fuel-efficient technologies and infrastructures to meet these goals [12,15].

Out of the above pathways, this study focuses on alternative aviation fuels and specifically non drop-in fuels, namely fuels that, due to their dissimilar properties (heating value, atomization, density, etc.) compared to conventional jet fuel, require alterations on the fuel delivery systems, fuel tanks, injectors and other infrastructure. According to the road-map towards carbon neutrality [1,12], non-drop in fuels, such as Liquefied Natural Gas (LNG), are placed as a mid-term solution, while liquefied hydrogen and battery-assisted flight finally dominate in the long term [6,16]. The near-term solution of bioenergy-derived kerosene (also known as bio-kerosene) is credited with the ability to decrease net CO_2 emissions up to 80% within its life-cycle [1–3,11] and is already certified for use on commercial flights when blended with fossil kerosene [11,15,17,18]. A comparison between the more technologically mature bio-kerosene and non drop-in fuels would hold more interest from a techno-economic or life-cycle perspective. However, this falls outside the scope of the current research, which focuses on evaluating non-drop-in fuels in current aero-engines and advancing the corresponding simulation methods required to achieve this.

A recent study [19] tackles the integration of LNG in aviation by evaluating the mission of retrofitted aircraft, so as assess the trade-offs between energy consumption and CO_2 emission per range unit by taking into account only its different heating value, density and pre-calculated Emission Indexes (EIs). Another approach [20] extends even further by re-designing the engine cycle according to aircraft thrust requirements and running an aircraft mission analysis for a plethora of alternative fuels, representing each main fuel family (i.e., methane for alkanes, butanol for alcohols, bio-kerosene for drop-in SAFs, etc.). A different approach [21] suggests, via simulation, a novel propulsion system of a turbofan coupled with a fuel cell to power the aircraft's auxiliary power unit in order to evaluate performance enhancement and CO_2 reductions, with respect to only the design operating conditions when utilizing non-drop-in fuels including hydrogen, methane, methanol, ethanol, dimethyl ether and their blends.

LNG offers several advantages and drawbacks as an aviation fuel. One of its key benefits is its ability to generate about 20% less CO_2 emissions for the same heat output compared to conventional jet fuel. It is also economically feasible when derived from fossil sources due to the vast natural gas reserves and low production costs, making it a viable alternative aviation fuel [1,19]. Additionally, LNG has a higher specific energy density, leading to reduced fuel consumption. However, LNG has notable drawbacks. Its low volumetric energy density necessitates larger storage tanks, which is challenging in the limited space available on aircraft. Significant infrastructure investments are required for airports, including LNG storage tanks, liquefaction facilities, and refueling pipelines. LNG's reactive nature also introduces safety concerns, particularly in crash scenarios. Furthermore, using LNG increases the aircraft's tank weight and drag, leading to a 7–10% rise in energy consumption according to respective literature [19].

MeOH, on the other hand, is one of the most commonly produced chemicals with a broad range of applications [22]. While it is not widely used directly as aviation fuel, it mostly serves as feedstock to produce synthetic kerosene [1]. MeOH can be synthe-

sized from fossil sources or biogenic materials, offering potential life-cycle CO_2 reduction, depending on the methods used for hydrogen production and CO_2 sourcing [1,22,23]. Combustion of MeOH emits 5.5% less CO_2 than kerosene for the same energy output while offering significant emission reduction potential such as NO_x by 75–90% and particulate matter emissions by 50% in certain applications [10,24,25]. Its high vaporization heat also lowers the post-combustion temperature of a gas turbine powerplant, reducing thermal NO_x formation and potentially enhancing turbine lifespan [24,25]. Despite these advantages, MeOH has several drawbacks. Its low specific energy density requires approximately twice more fuel mass flow compared to kerosene for the same net thrust which, when coupled with its low volumetric energy density, causes increased size and weight requirements for the aircraft, engine and wings, making the aircraft mission much more energy consuming [1]. Retrofitting propulsion systems for MeOH use requires specialized injectors and more energy-intensive pumps to handle the increased fuel workload and compensate for methanol's low lubricating properties [22,23,25]. Therefore, is a highly toxic and corrosive fuel, which necessitates the use of specialized storage containers and strict safety measures for its handling. Furthermore, methanol is only poorly miscible with kerosene, making it unsuitable for blending [25]. While MeOH shows promise in reducing emissions, its usefulness in aviation remains under-explored, and further research is needed to fully assess its potential.

While the aforementioned computational studies provide valuable insights into the integration of non drop-in fuels, they assume that the combustion process remains unaffected by changes in engine design or fuel type. To evaluate emissions within the design space, these studies rely on either fixed Emission Indices (EIs) or simple (one-reaction) stoichiometric calculations, neglecting potential fluctuations in combustion efficiency. As a result, they are unable to fully quantify key aviation pollutants such as NO_x, CO and UHC, leaving gaps in understanding the environmental impacts of such fuels. Other studies [26–30] focus on accurately predicting combustion and post-combustion properties (e.g., emissions, ignition delay time, flame speed) of alternative fuels by employing state-of-the-art physics-based tools using detailed chemical and thermodynamic calculations. Addressing this gap, the current study proposes integrating advanced 0-D turbomachinery component models [31] with a physics-based Chemical Reactor Network (CRN) model for isobaric gas turbine combustors [30] within a unified simulation framework. This framework ensures transparency, seamless intercommunication between tools, and ease of use. The proposed model is applied to evaluate the performance and emission characteristics of a modern Geared Turbofan (GTF) engine powered by two liquid non-drop-in fuels: LNG and methanol (MeOH).

The engine model developed in this study is first applied and adapted to the layout of a current generation GTF. Once validated, the adapted model is used to simulate the performance of the aforementioned non-drop-in fuels. Initial simulations assume the same output thrust conditions as those of the engine's baseline Jet-A operating conditions. Subsequently, simulations are performed under set turbine inlet temperature (TIT) conditions matching the baseline, thereby expanding our understanding of the engine's operating limits and its associated emissions. Finally, a real mission scenario within the operational scope of the studied engine is simulated to demonstrate that the advantages of these fuels persist under actual flight objectives and constraints.

2. Methodology

In this section, the assumptions made, the numerical methods used, the proposed model concept, virtual structure and configuration are discussed.

2.1. Engine Performance Model

To analyze the impact of alternative fuels on current aeroengines, a general model of a high-bypass, dual-spool, axial-flow, geared turbofan (GTF) engine [32] is generated in the PROOSIS v6.2.0 object-oriented gas-turbine simulation environment [33]. The engine consists of the following components and each of them is separately modeled and coupled accordingly within the PROOSIS framework as illustrated in Figure 1:

- Inlet Duct (InEng);
- Fan (CmpFan)— A single-stage fan;
- Gearbox (GearFan)—Transmits torque from the low-pressure compressor to the fan with a gear ratio of approximately 1:3 and an assumed mechanical efficiency of 99.5%;
- Low-Pressure Compressor (CmpL)—A three-stage compressor;
- High-Pressure Compressor (CmpH)—An eight-stage compressor;
- Combustion Chamber (Brn)—An isobaric TALON X burner [34];
- High-Pressure Turbine (TrbH)—A two-stage cooled turbine that drives the high-pressure compressor;
- Low-Pressure Turbine (TrbL)—A three-stage turbine that drives the fan and the low-pressure compressor;
- Primary Nozzle (NozPri)—A fixed-geometry convergent nozzle that directs the main exhaust stream;
- Bypass Nozzle (NozSec)—A fixed-geometry convergent nozzle that directs the bypass air stream.

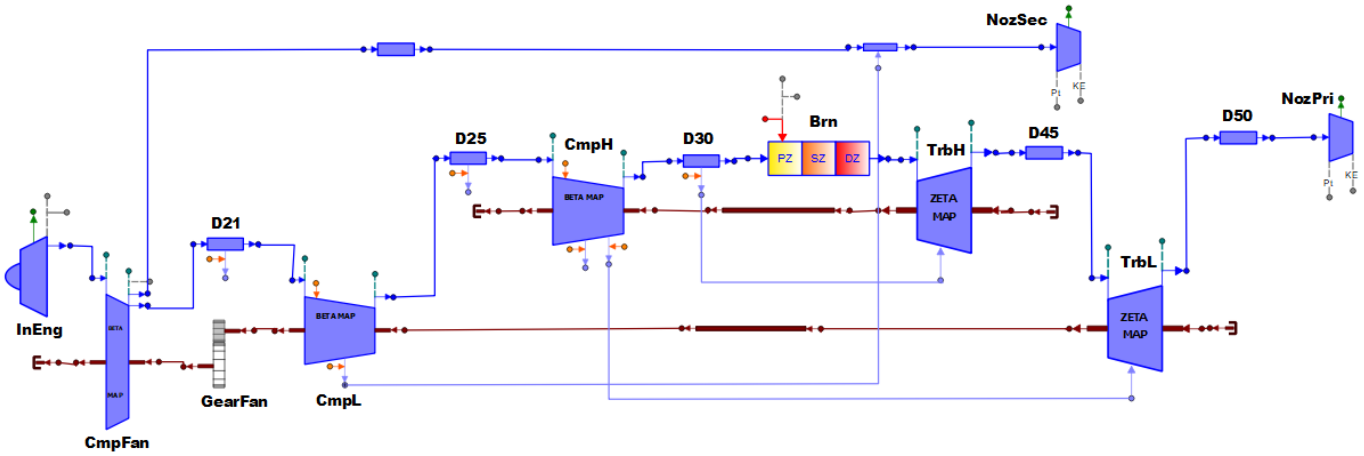

Figure 1. GTF engine model schematic. The interconnecting ducts (D) are labeled according to the engine station numbering, which is consistently followed from this point onward.

The novelty of the proposed engine model compared to previous respective attempts which utilize empirical algebraic models to estimate emissions and combustion efficiency [31] is that it incorporates a physics-based 1-D combustor model. According to the literature [26,27,30], such models are essential to provide deeper insights into the combustion characteristics and pollutant formation mechanisms of less-studied fuels compared to conventional Jet-A, such as MeOH and LNG. All the other components of the engine seen in Figure 1 are sourced from the TURBO library [33] of the environment.

2.2. Combustor Model

The model used is a three sub-volume generalist model of an isobaric combustor [30] which is developed and tested by LTT/NTUA in the CANTERA environment [35]. It is introduced for the first time in the PROOSIS framework, to work in unison with the other component models. To accomplish this, the common C++ interface between the two software platforms is employed, enabling the burner's main C++ function to be

defined externally while remaining accessible within the PROOSIS environment. This shared function serves as foundation for the construction of the CRN burner component in PROOSIS, represented as "Brn" in Figure 1.

The division of the combustor volume into zones, along with the corresponding interconnections between these zones, creates a Chemical Reactor Network (CRN), illustrated in Figure 2, which is also used to reference the model. The latest version of the utilized CRN model, though following the same principal modeling strategy of Primary, Secondary and Dilution zone partitioning of the burner, has a slightly altered structure, giving it the ability to include water vapor inflow, which is modeled separately than the dry air intake. Also, computational time is reduced to less than a third of the time needed by the initial version, as discussed in [30]. This is achieved by introducing a dynamic initialization mixture within each zone, which is forced to react at the start of the simulation, accelerating the convergence of the integral solution.

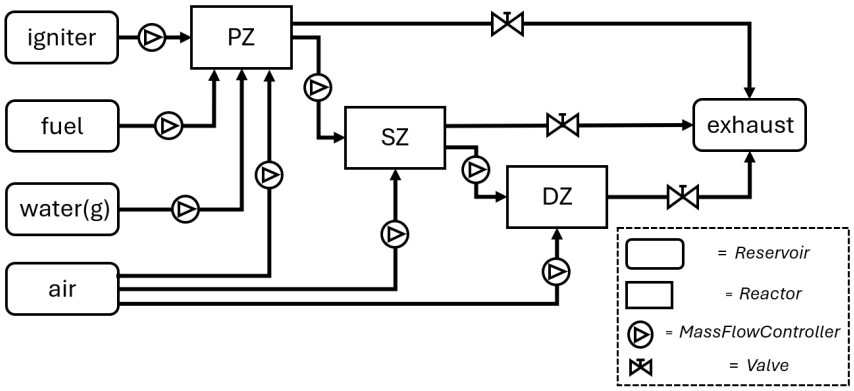

Figure 2. Virtual architecture of the CRN isobaric combustion chamber model.

The fuel information required by the model to simulate a specific fuel comes in the form of a combustion kinetic mechanism (defining a range of possible reactions among a specific set of potential species) as well as the assumed composition of the fuel. For the applications discussed in this work, any information about the fuel-combustion mechanisms and the assumed fuel compositions are disclosed in Table A1 of Appendix A and further explained.

Additionally, typical 0-D engine PROOSIS models rely on precomputed 3-D interpolation tables of thermodynamic data to simulate the effects of different fuels on exhaust gases. These tables are generated using NASA-CEA 2 software [36] and integrated into the model as working medium model. The current engine model follows this approach for all components except the CRN burner, which operates independently of this working medium model.

2.3. Combustor Model Parameter Adaptation

Separately, yet following the same adaptation principles, the CRN model of the burner has a number of geometric and flow parameters which are user-defined so as to produce more accurate emission estimations of the engine in question. The geometric parameters, specifically the length L and the reference area A_{ref} of the combustor, together with the length ratios of each zone (LR_{PZ}, LR_{SZ} and LR_{DZ}) are either known or easily estimated.

Meanwhile, the ratios of the core airflow (ARs) entering each zone or equivalently the equivalence ratio (ϕ) in each zone (given that they are explicitly linked) are often a priori unknown and thus usually serve as Design Variables (DVs) within the adaptation process in order to minimize the discrepancy between the model emission estimations and their known values. These parameters determine the quality of combustion in each zone of the burner, highly influencing the post-deflagration temperature and the formation

of pollutants [30]. Yet when using the CRN model in question, two distinct assumptions for these parameters can be made. The first, which is also used in the introductory study concerning the model [30], states that the AR of each zone is considered unaffected by the operating conditions and thus the equivalence ratio of each zone accordingly altered with respect to changes in Fuel-to-Air Ratio (FAR). The second assumes that the different ϕ values of each zone are kept constant within the whole operating range of the engine, thus modifying the ARs accordingly to achieve this. Which of the two assumptions better reflects the operation of the current burner is examined in more detail in Section 3.2.

The implemented adaptation flow chart is illustrated in Figure 3, while the Objective Function (OF) is formulated as follows:

$$OF = \sum_i \omega \left(1 - \frac{EI_{NOx}^{(i)}}{EI_{NOx}^{(ref,i)}}\right)^2 + (1-\omega)\left(1 - \frac{EI_{CO}^{(i)}}{EI_{CO}^{(ref,i)}}\right)^2, \quad i = \{TO, Cl, App, Id\} \quad (1)$$

where a choice for $\omega = 85\%$ is made in order to place more emphasis on NO_x accuracy.

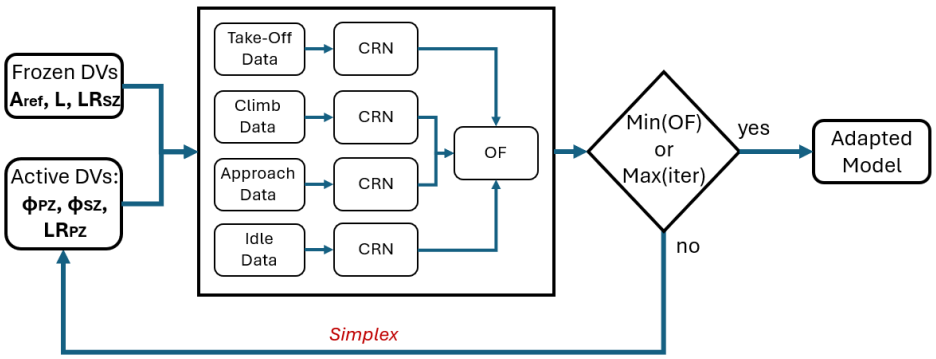

Figure 3. CRN model adaptation loop.

3. Application Test Case

A contemporary GTF engine, the Pratt and Whitney PW1127G-JM engine, is selected to be simulated using the general GTF model. Enough engine-specific experimental and geometric data are available to enable the model's adaptation. A blueprint of the engine's cross-section can be found in literature [32], while its fan diameter and length are known to be 2.10 m and 3.08 m, respectively. This engine powers the Airbus A320neo and was first introduced in January 2016. It is a high-bypass, dual-spool, axial-flow geared turbofan engine.

Fuel and exhaust emission data are procured from the ICAO Aircraft Engine Emissions Databank [37] as well as the Overall Pressure Ratio (OPR) and the Bypass Ratio (BPR) of the engine at ICAO Take-Off (TO) conditions. These measurements pertain to an engine mounted on a test rig configuration and tested under static atmospheric conditions at sea level. All operational parameters of the GTF under consideration constitute the assumed reference operating conditions of this study and are presented in Table A2, Appendix B.

The general twin-spool geared turbofan achitecture of Figure 1 is adjusted to simulate the specific PW1127G engine by a process of minimizing deviations between the model-computed net thrust (F_n) and fuel mass flow ($\dot{m}_f$) and their reference values of Table A2 by modifying design point parameters and locally adapting the maps of the turbo-machinery components.

3.1. Engine Cycle

In Figure 4, the ICAO operating line, also known as the net thrust and Thrust Specific Fuel Consumption (TSFC) correlation, is shown as computed by PROOSIS, with thrust

varying by approximately 2.5% in each calculation. The four discrete reference operating points are displayed along with their deviations from their respective calculated values. Figure 4 also includes the deviation from the reference performance parameters (OPR, BPR, $\dot{m}_f$) corresponding to the TO thrust of 120.43 KN (see Table A2), which serves as the design point of the PROOSIS model.

The maximum deviation at the design point is around 0.4%, while across the entire range of operating conditions, it remains below 3%. The model is thus considered certified in accordance to the values provided by ICAO.

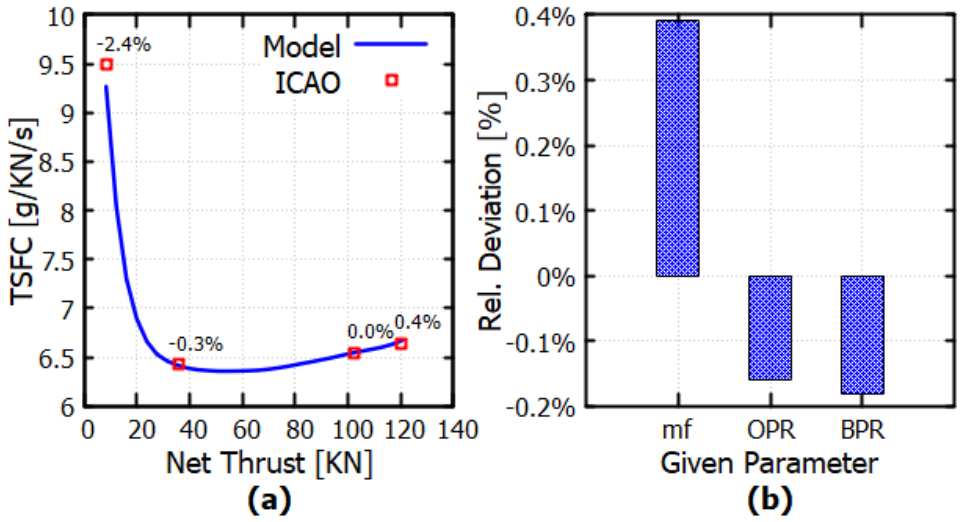

Figure 4. Engine model verification: (**a**) comparison of model-estimated operating line and ICAO-given operating points along with relative variation of the line with respect to each point, (**b**) design point model-estimated parameter variation with respect to ICAO-given values.

Total pressure, total temperature and core airflows of the simulated and verified GTF/Jet-A engine cycle are presented in Figure 5 per engine station in order to serve as a baseline cycle reference for the alternative fuel evaluations of Section 4.

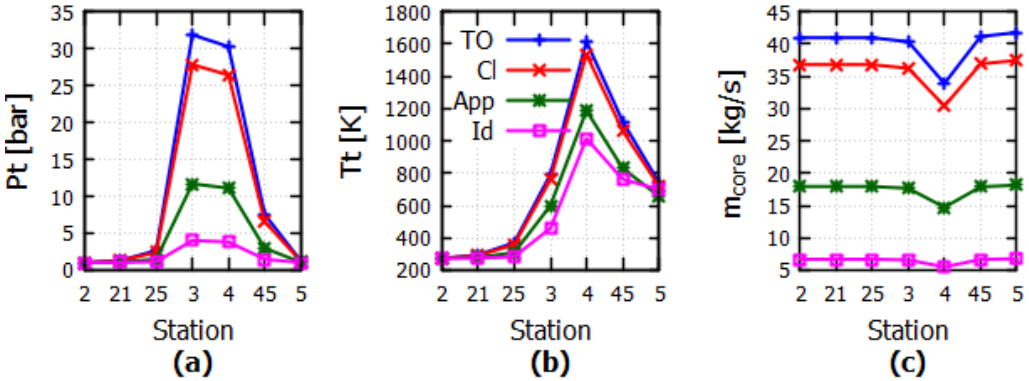

Figure 5. Total pressure (**a**), temperature (**b**) and core mass flow (**c**) of Jet-A-powered GTF engine (baseline operation) for 4 operating modes (station numbering according to Figure 1).

3.2. Combustor and Emissions

First, the constant CRN parameters (L, A_{ref}, LR_{SZ} and LR_{DZ}) are deduced by knowing the GTF's length and fan diameter and assuming its cross-section (found in [32]) is drawn in scale. Second, for the adaptation process to better represent the physics of the combustor design, the correct assumption has to be made concerning the combustion process.

According to the documentation of engine's burner, referred as the TalonX combustor, it cannot be modeled with the first approach mentioned in Section 2.3, given that its low

NO_x design uses special High Shear swirlers that uniformly create a fuel-rich mixture ($\phi_{PZ} > 1$) within the PZ by changing the swirl angles of the two swirling air passages and the air flow split between them [34]. The family of burners working with this general principle is referred to as Rich-Quench-Lean, a.k.a. RQL for short, and are represented in Figure 6a. Thus, the initial combustion occurring in the PZ is conducted within the low-NO_x-formation-rich region of ϕ, while downstream of the PZ, the flue gasses are quenched and diluted by the SZ and DZ air flows, decreasing the global ϕ towards its lean region along with their mean-adiabatic temperature T_{ad}. This trend is qualitatively recreated using the CRN model for the current burner by varying the ϕ_{PZ} through adjustments to the ARs entering each zone (T_{t3}, p_{t3} & $FAR = const.$). The effects on EI_{NOx} and T_{ad} are depicted in Figure 6b to further ensure the model's validity.

Figure 6b, consistent with related literature [6,38], shows that the peak of T_{ad} slightly differs from the peak of NOx with respect to ϕ, as they appear on opposite sides of the $\phi = 1$ line. This trend is expected to be within the predictive ability of the utilized Jet-A combustion mechanism (see Appendix A), which accounts not only for thermal NO_x but also for the prompt NO_x and N_2O pathways. These pathways play a significant role in NO_x formation in the $\phi < 1$ region, leading to the observed optimum in Figure 6b.

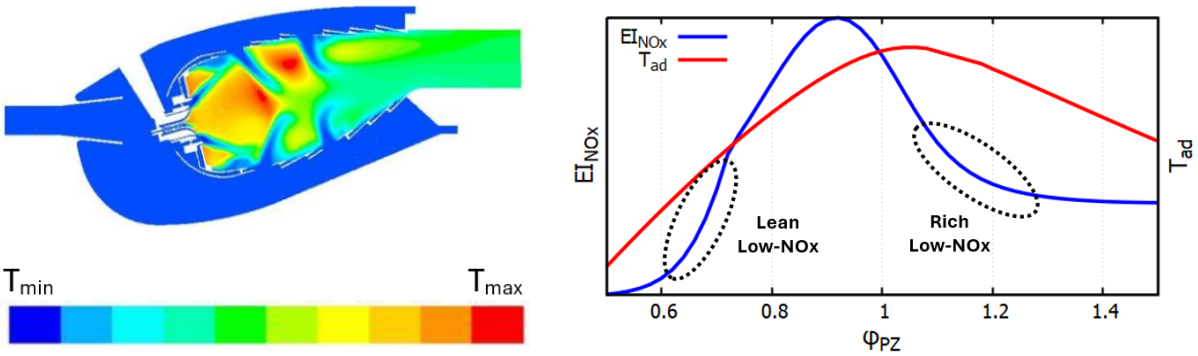

(**a**) (**b**)

Figure 6. TalonX characteristics. (**a**) RQL burner-family cross-section with qualitative temperature contours [39]. (**b**) Qualitative EI_{NOx} & T_{ad} vs ϕ_{PZ} map for the TalonX at TO conditions.

Assuming that the TalonX burner can maintain constant ϕ values per zone throughout its operational range, the second approach is followed. Therefore, the ϕ_{PZ} and ϕ_{SZ} along with the LR_{PZ} are considered active DVs of the adaptation/optimization process visualized in Figure 3, while L, LR_{SZ} and A_{ref} are deemed frozen DVs.

The adaptation results of the CRN model are shown in Figure 7. Specifically, the initial and adapted CRN-derived results for EI_{NOx}, EI_{CO}, EI_{UHC}, and EI_{CO_2} profiles, relative to the engine's net thrust, are compared against the corresponding four reference operating points (TO, Cl, App, Id). Both initially and finally selected DVs of the adaptation process of Figure 3 are included in Appendix C and remain unchanged after the adaptation for the following calculations.

Figure 7 demonstrates that the engine model effectively captures the true emission trends across the entire operational range, akin to the validation of the working line accuracy discussed previously. The adaptation successfully achieved to improve the estimation of EI_{NOx} by making trade-offs with the EI_{CO} predictions, which is expected given that NO_x formation is inversely proportional to unburnt particle formation such as CO [38]. It is worth noting that the relatively low differences between the final and initial DVs (see Table A3 of Appendix C) indicates that the adaptation effectively preserves the physical characteristics of the combustor in question. Also, for the current adjusted configura-

tion, the model seems unable to yield accurate EI_{UHC} estimations, neither qualitative nor quantitative and therefore such predictions are not included in the later parts of this work.

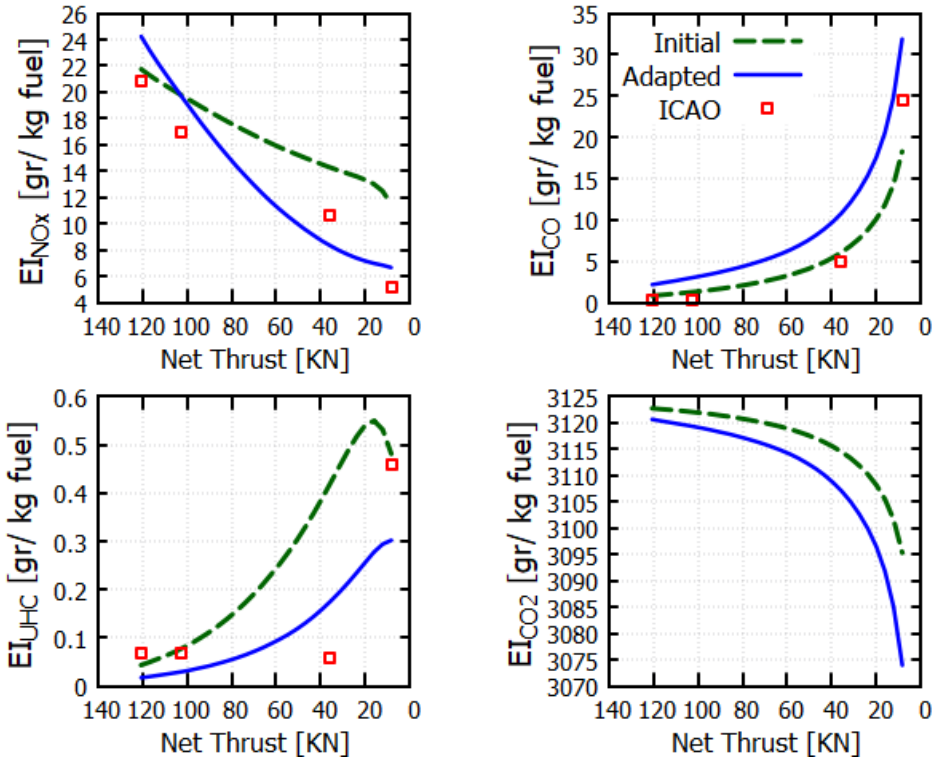

Figure 7. GTF model results: comparison between initial, adapted and ICAO (if available) NO_x-CO-UHC-CO_2 emission values with respect to engine thrust.

Furthermore, LTO emission comparisons are meant to highlight the joint accuracy of cycle and emission predictions, given that they are calculated using $\dot{m}_f$ and EI estimations as in Equation (2):

$$LTO_k\,[g] = \sum_i 60\,\dot{m}_{f,i}\,t_i\,EI_{k,i}, \quad i = \{TO, Cl, App, Id\}\ \ \&\ \ k = \{NO_x, CO\} \tag{2}$$

where $t = \{0.7, 2.0, 4.0, 26.0\}$ min is the time spent by the aircraft in each of the TO, Cl, App and Id operating modes, respectively.

The LTO NO_x and CO emissions of the GTF model are shown in Figure 8. Both prediction evaluations clearly demonstrate the qualitative reliability of the presented model in estimating NO_x and CO emissions, with discrepancies of 11% and 33%, respectively. This capability was previously demonstrated by the authors for the standalone CRN model [30], but it has now been extended for use as part of a complete aero-engine model, fully integrated within the PROOSIS framework. It should be noted that the quantitative predictive accuracy for NO_x is significantly better compared to CO. Nonetheless, the PROOSIS/CRN model can still be utilized to assess emission performance by slight overestimation given that its overall fidelity is deemed sufficient for a 0-D engine model.

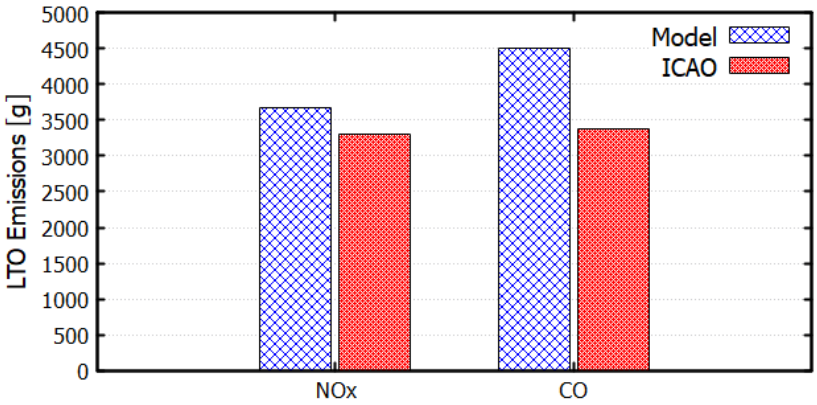

Figure 8. Calculated (model) and reference (ICAO) LTO NO_x and CO emitted mass comparison.

4. LNG and MeOH Evaluation

The calibrated GTF model is employed to evaluate the use of MeOH and LNG on the engine in question. Each fuel has physical and chemical properties that differentiate it significantly from typical jet fuel as shown in Table 1, those most concerning this work being Lower Heating Value (LHV) and latent vaporization heat.

Table 1. Properties of simulated fuels.

Properties	Jet-A	LNG	MeOH
Chemical formula	$C_{11}H_{21}$ *	CH_4, C_2H_6, C_3H_8	CH_3OH
Density [kg/m^3]	775–840 (at 15 °C)	420–470 (at −160 °C)	798 (at 15 °C)
Lower heating value [MJ/kg]	42.8–43.2	48–55	20.09
Latent heat of vaporization [kJ/kg]	250	510	1100
Freezing point [°C]	−47	−182.2	−97.6
Autoignition Temperature [°C]	255	535	465
Min. Autoignition Energy [MJ]	0.25–0.4	0.28–0.30	0.21

* an approximate formula [38], Jet-A is a varying HC mixture consisting mostly of paraffins. (n- and iso-alkanes), napthalenes and aromatic HCs [38,40] (more in Appendix A).

Given that both alternative fuels have lower carbon content and higher vaporization heats than Jet-A, they are anticipated to reduce the cycle maximum temperature and the overall engine emissions for the same thrust level attained with Jet-A; set-F_N. Also, compared to Jet-A, LNG's higher LHV implores a decrease in fuel flow, while MeOH's lower LHV indicates the opposite. This initial evaluation involves comparisons of fuel consumption, Turbine Inlet Temperature (TIT), rotational speed (N) and emission results (including both EI and LTO calculations). Furthermore, variations of the cycle temperature, pressure and core airflow per station for each fuel are analyzed to better understand their overall impact on engine performance. The set-thrust approach evaluates the ability of the studied fuels to meet the propulsive requirements of the current aircraft design, thus assuming their conceptual application in the current aircraft fleet.

Subsequently, the LNG and MeOH are evaluated and compared in the same manner, but this time under the assumption that the same TIT as the baseline Jet-A operation is maintained. This analysis, referred as set-TIT approach, serves to enhance our understanding of the expansion of current technological capabilities of aero-engines when fueled by LNG or MeOH. It assumes that retrofitting requirements for such fuels affects the propulsive needs

of the existing fleet [1,19]. Thus, this analysis opts to provide insights into the adaptability of current engine technology to alternative fuels.

In both evaluations, it is assumed that the CRN burner model configuration remains the same according to the adaptation process followed in Section 2.3, meaning that the zones of the model are expected to operate at the adapted ϕ conditions, regardless of the fuel used. This assumption is based on the premise that the TalonX operation remains consistent and adapts to the new fuels in a similar manner as it does to Jet-A, given that no specific information is provided for the burner for LNG or MeOH-powered operation.

4.1. Set-Thrust Operation

The set-F_N condition denotes the possibility of operating current engines using LNG or MeOH with minimized changes in the engine cycle and aircraft infrastructure, assuming alterations be limited to the aircraft's fuel storage and supply systems. Thereby, the set-F_N approach constitutes a more conservative alternative fuel evaluation scenario. The main thermodynamic and emission parameters yielded from this analysis are shown in Table 2.

Table 2. LNG and MeOH evaluation in GTF requesting the same net thrust as the baseline Jet-A operation of the GTF.

	Take-Off	**Climb**	**Approach**	**Idle**
F_N [N]	120,430.0	102,365.5	36,129.0	8430.1
		Jet-A (baseline)		
$\dot{m}_f$ [kg/s]	0.803	0.670	0.232	0.078
TIT [K]	1614.44	1535.39	1188.18	1013.96
N_H [rpm]	20,649	19,948	15,776	11,343
N_L [rpm]	8848	8286	5193	2620
EI_{NOx} [g/kg]	24.22	19.68	8.36	6.66
EI_{CO} [g/kg]	2.02	2.82	10.02	30.02
EI_{CO_2} [g/kg]	3120.65	3119.33	3107.27	3073.95
		LNG		
$\dot{m}_f$ [kg/s]	0.707	0.590	0.204	0.069
TIT [K]	1592.25	1515.58	1177.64	1006.24
N_H [rpm]	20,660	19,960	15,781	11,344
N_L [rpm]	8855	8293	5195	2621
EI_{NOx} [g/kg]	11.18	9.31	5.60	5.86
EI_{CO} [g/kg]	1.35	1.88	7.09	20.50
EI_{CO_2} [g/kg]	2781.47	2780.64	2772.42	2751.34
		MeOH		
$\dot{m}_f$ [kg/s]	1.644	1.373	0.477	0.161
TIT [K]	1547.28	1475.73	1155.01	988.37
N_H [rpm]	20,660	19,976	15,785	11,338
N_L [rpm]	8855	8293	5196	2621
EI_{NOx} [g/kg]	4.28	3.48	1.50	1.09
EI_{CO} [g/kg]	0.75	0.99	3.17	8.69
EI_{CO_2} [g/kg]	1370.52	1370.13	1366.68	1357.99

For the same thrust, LNG fuel consumption drops by approximately 12%, while MeOH produces a fuel flow increase by 105%, a finding also observed in [19,24,25]. TIT is lowered for both fuels, yet the greatest decrease of 2.5–4% is observed for MeOH. Both aforementioned trends are visualized in Figure 9. As stated above, the heat of vaporization, being greater than Jet-A in both fuels, causes the TIT drop, thus indicating the potential of improving the engine life expectancy. Yet the cooling advantage of MeOH lies also in

its lower LHV, which causes more fuel mass to be injected into the burner, which in turn requires even more heat to ignite.

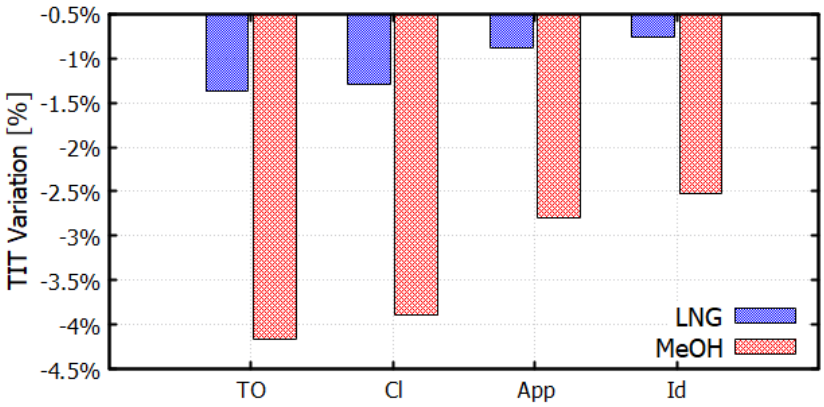

Figure 9. Set-thrust: TIT variation of LNG and MeOH-powered GTF, relative to its baseline Jet-A operation.

The decrease in all post-combustion temperatures (Stations 4, 45, 5) caused by both fuels can be observed also in Figure 10, where the covered cycle parameter variations relative to GTF/Jet-A operation are displayed, yet only for the Take-Off and Idle (Id) modes, given that they constitute the boundaries of possible variation. Figure 10 shows the aforementioned total mass-flow differentiation induced by each fuel due to their heating properties. Since the rotational speeds of both the high and low pressure spools remain virtually unchanged (see Table 2), the relatively minor variations in the engine's baseline total pressure profiles are reasonable.

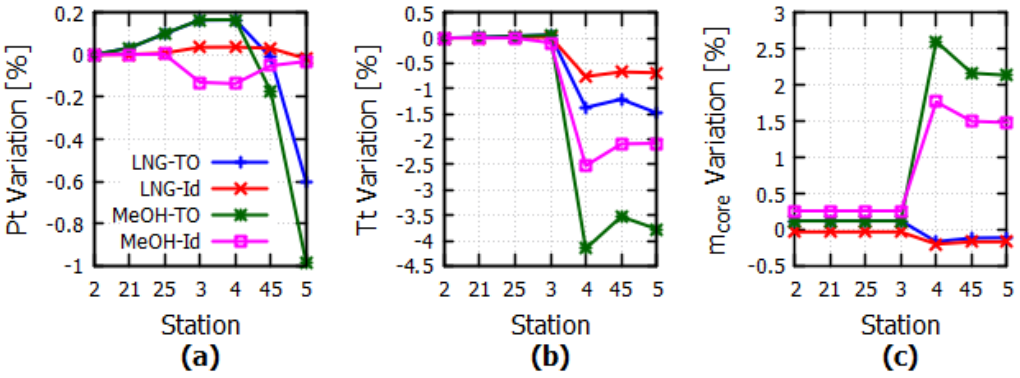

Figure 10. Set-thrust: total pressure (**a**), temperature (**b**) and core mass flow (**c**) relative variation of LNG and MeOH-powered GTF, for TO and Id operating modes.

Regarding the EIs covered in Table 2, both fuels severely reduce emissions for the same thrust setting. Examining only the EIs indicates that MeOH shows a clear advantage over LNG when it comes to curbing of pollutant emissions. Yet when analyzed as part of the engine LTO cycle for each fuel, the results differ, because the variation of $\dot{m}_f$ and the time of each phase play a significant factor as well, according to Equation (2). The increase in fuel consumption of MeOH, presented in Table 2, plays a significant factor in the LTO emitted mass of pollutants shown in Figure 11. Specifically, the CO_2 reduction potential of LNG is about 21%, while MeOH's potential amounts to 10%, always relative to the GTF/JetA results of the model, presented in Figure 8. In contrast, MeOH clearly displays the capability to reduce LTO NO_x by 64%, thus overcoming the LNG's potential of 48%, proving that when it comes to NO_x the EI reduction prevails over the increase in fuel flow. The emitted mass of LTO CO remains practically the same for both fuels.

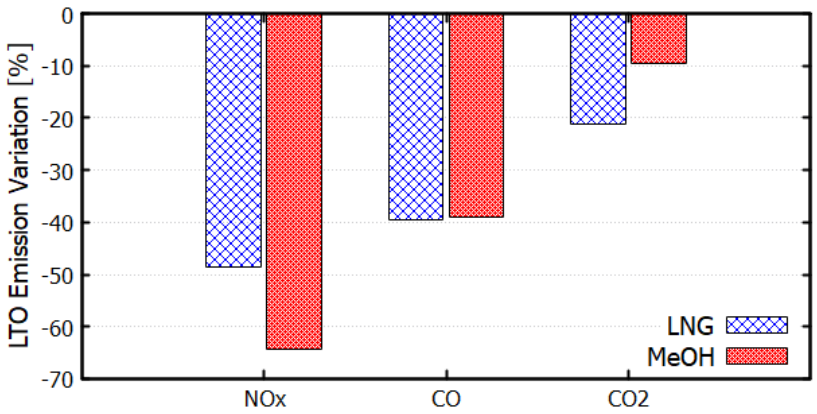

Figure 11. Set-thrust: LTO NO_x, CO and CO_2 variation of LNG and MeOH-powered GTF, relative to its baseline Jet-A operation.

4.2. Set-TIT Operation

Having shown that the GTF can produce the desired thrust using MeOH and LNG while reducing post-combustion temperatures, the potential for producing more thrust than the Jet-A operation comes into question. More importantly, the thrust-increasing potential is expected [24,25] and should be quantified for the current aero-engine, along with assessing its influence on emission and other cycle parameters. The results of the evaluation approach in question for LNG and MeOH are displayed in Table 3 (the baseline Jet-A operation is the one shown in Table 2). Idle is excluded from this analysis, as there is no practical need for additional F_N for this operating regime.

Table 3. LNG and MeOH evaluation in GTF requesting the same TIT as the baseline Jet-A operation of the GTF.

	Take-Off	**Climb**	**Approach**
TIT [K]	1614.44	1535.39	1188.18
		LNG	
$\dot{m}_f$ [kg/s]	0.737	0.621	0.213
F_N [N]	124,606.6	107,319.3	37,639.4
N_H [rpm]	20,857	20,138	15,917
N_L [rpm]	8969	8460	5294
EI_{NOx} [g/kg]	11.73	9.77	5.63
EI_{CO} [g/kg]	1.23	1.73	6.81
EI_{CO_2} [g/kg]	2781.67	2780.88	2772.86
		MeOH	
$\dot{m}_f$ [kg/s]	1.871	1.601	0.542
F_N [N]	132,755.7	117,779.7	41,317.9
N_H [rpm]	21,231	20,545	16,249
N_L [rpm]	9178	8779	5527
EI_{NOx} [g/kg]	4.97	4.15	1.60
EI_{CO} [g/kg]	0.57	0.78	2.80
EI_{CO_2} [g/kg]	1370.81	1370.46	1367.26

The initial research enquiry of this work is answered for both fuels and is visualized in Figure 12. LNG is capable of increasing net thrust by 3.5% for TO to 5% for Climb (Cl) operation, while still consuming 8–7% less fuel mass than Jet-A, respectively. Furthermore, MeOH can boost net thrust by up to 10% during TO and 15% during Cl while also leading to a 132–138% increase in fuel consumption, respectively.

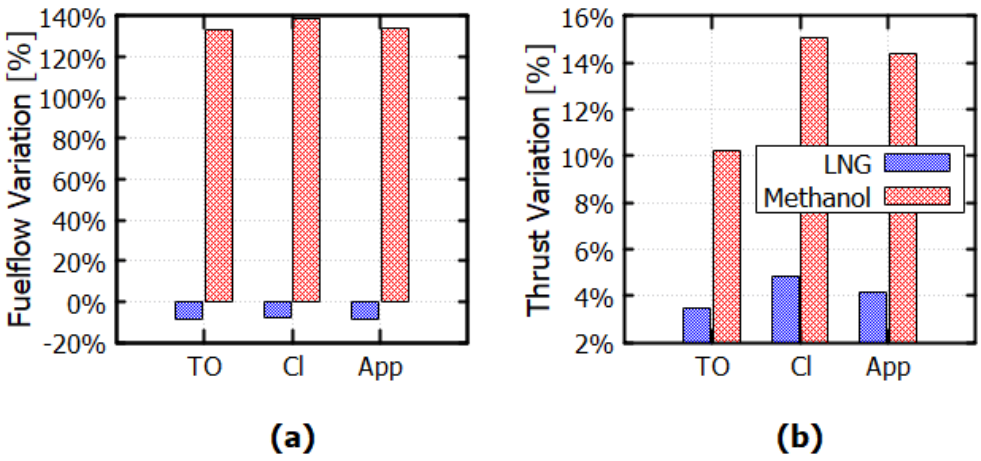

Figure 12. Set-TIT: fuel massflow (**a**) and thrust (**b**) variation of LNG and MeOH-powered GTF, relative to its baseline Jet-A operation.

By further examining the cycle parameter variations in the TO and Cl modes displayed in Figure 13, the cycle parameter trends are similar for both fuels but more emphatic for MeOH. It can be deduced that both fuels lead to a significant increase in core airflow (2–10%) before combustion, indicating that more air is drawn into the engine's intake. This is accompanied by a rise in the overall pressure ratio (OPR) and the expected temperature increases at Stations 25 and 3. The resulting increase in the load on the compressor components, which is primarily responsible for the thrust augmentation, may necessitate modifications to the compressor block, such as a proportional increase in size. This is also expected to result in an increase in engine dry weight, a conclusion similarly highlighted in [1] for ethanol, a closely related but distinct alternative aviation fuel. For both fuel types, the additional fuel required to meet the set-TIT condition results in a 1–6% increase in rotational speed, as shown in Figure 14. This change in power plant operation reasserts the previous statement as higher rotational speeds could negatively impact engine lifespan and should be thoroughly assessed. Also, the increased $\dot{m}_f$ (see Figure 12) causes exhaust gases with greater specific heat capacities to pass through the turbine [20]. This in turn leads more energy to be recuperated from the turbines and transferred to the compressors working at greater speeds, thus causing airflow and compression ratio to increase. This trend applies to both fuels across all studied modes but is more pronounced for MeOH, particularly during Cl due to its significant increase in $\dot{m}_f$.

Finally, the emission assessment shows a slightly smaller reduction potential for all studied pollutants from an EI perspective (see Table 3). Yet, once again, the LTO calculations for NO_x, CO and CO_2 presented in Figure 15 indicate otherwise. LNG overall keeps its LTO decreasing ability, though slightly mitigated. It is clear that in the equal-TIT condition, MeOH loses its GHG reduction potential, given that the CO_2 emitted mass for MeOH rises by 10% compared to Jet-A, predominately due the greatly increased Idle fuel consumption given that the aircraft spends the most time in that phase. Otherwise, for MeOH, the LTO emitted mass of CO remains virtually unchanged, while its NO_x reduction ability remains more potent than LNG.

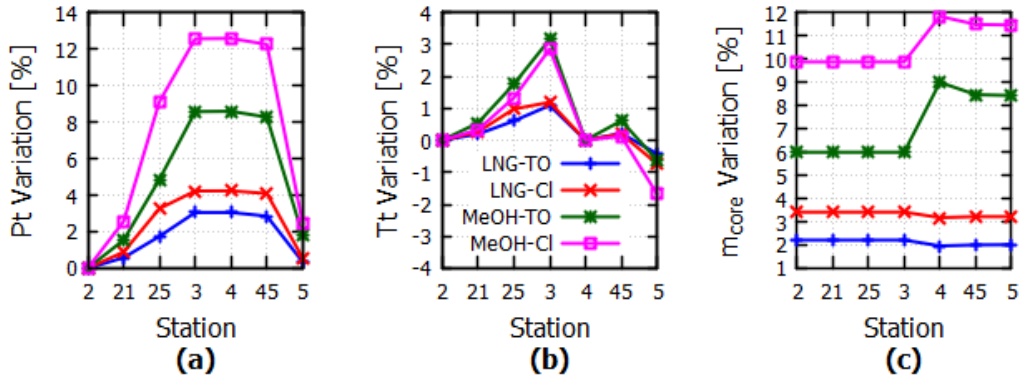

Figure 13. Set-TIT: total pressure (**a**), temperature (**b**) and core mass flow (**c**) relative variation of LNG and MeOH-powered GTF for TO and Cl operating modes.

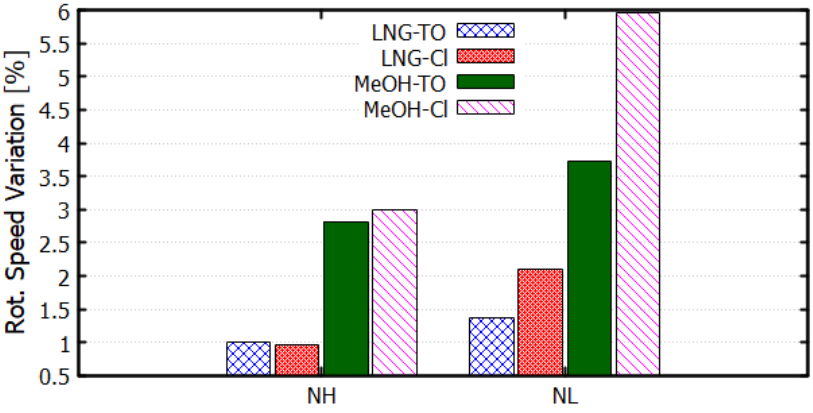

Figure 14. Set-TIT: low and high pressure spool speed variation for LNG and MeOH-powered GTF for TO and App operating modes.

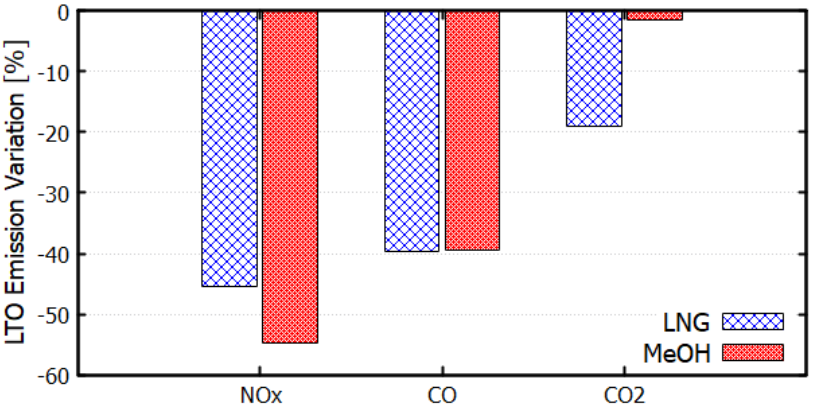

Figure 15. Set-TIT: LTO NO_x, CO and CO_2 variation of LNG and MeOH-powered GTF, relative to its baseline Jet-A operation.

4.3. Mission Analysis

The selected mission is meant to prove the mere feasibility of LNG- and MeOH-powered flight under simple weight restrictions of current aircraft, not to evaluate the mission-wise operational limits of the studied fuels, engine and aircraft. According to data from Eurocontrol, the average flight distance in Europe for 2019 (pre-pandemic) was 1062 km, while over 80% of flights departing from Europe (EU27 + U.K.) involved distances of up to 2000 km [41]. Therefore, different fuel scenarios are evaluated on an average real flight scenario from London to Barcelona, with a range of 1109 km. The flight model used to compute the mission parameters as well as the assumptions made for the aircraft

weights and retrofitting are discussed in Appendix D, by explaining the information of Figure A1. The mission profile specifics and flight route are presented in Figure A2 of the same Appendix. Additional aircraft data, such as aerodynamic parameters needed for mission analysis, are sourced from Base of Aircraft Data (BADA) [42].

The proposed GTF model is implemented to predict engine performance during flight by inputting the flight speed, altitude and net-thrust requirements of the mission. The emission evaluation of an aircraft during flight using engine-integrated detailed chemistry models, all executed within the PROOSIS environment, is also an important originality of this work. The mission analysis results are presented in Table 4 and Figures 16 and 17 covering variations in emission, net-thrust, Take-off Weight (TOW), total Fuel Weight (FW) and aircraft weight for each fuel scenario.

Table 4. Mission analysis aircraft and emission weight results.

Fuel	TOW [tn]	FW [kg]	CO_2 [kg]	NO_x [kg]	CO [kg]
Jet-A	62.35	4576.44	12,399.66	73.19	20.71
LNG	62.59	4048.16	9779.91	33.96	11.92
MeOH	67.40	9635.97	11,472.13	27.73	13.60

As established above, the low LHV of MeOH increases FW by 110% and TOW by 8%, since the payload and OEW remain the same for both fuels. In contrast, LNG reduces FW by 11.5% while increasing slightly TOW by 0.4% due to the increased OEW, which is caused by the LNG tank retrofitting assumption. However, the TOW and FW stay within the maximum allowable limit of 77 and 20 tons, respectively (see Appendix D), for both alternative fuels. This signifies that the flight with LNG and MeOH remains within the weight restrictions of the A320 for the mission in question.

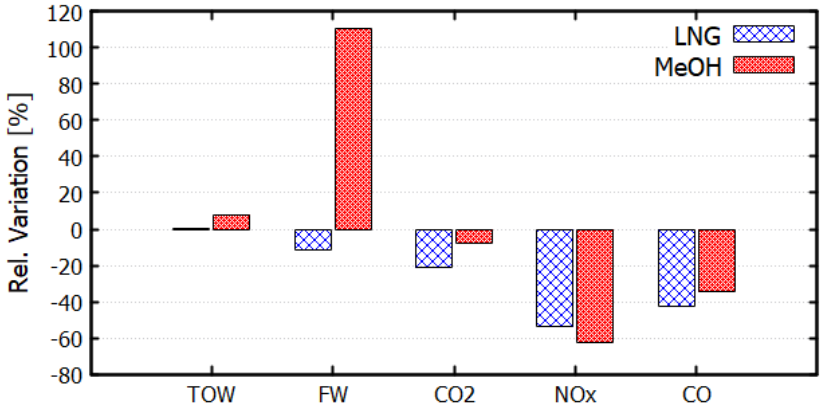

Figure 16. Mission analysis: comparison of aircraft TOW, FW and emission weight variations with respect to Jet-A operation, for LNG and MeOH.

Additionally, this specific flight scenario, under the assumptions made, grossly falls within the set-F_N category regardless of the fuel used, as indicated by the thrust time-series in Figure 17. This demonstrates that, for missions of comparable range, the set-F_N assumption is viable when evaluating MeOH or LNG for current aircraft. Finally, total CO_2, NO_x and CO emissions are all lowered by both fuels as illustrated in Figure 16. The trends of NO_x and CO EIs in Figure 17 once again appear to be inversely correlated. This observation is also supported by theory [38], which predicts a decrease in NO_x and an increase in CO during the progression of a typical mission.

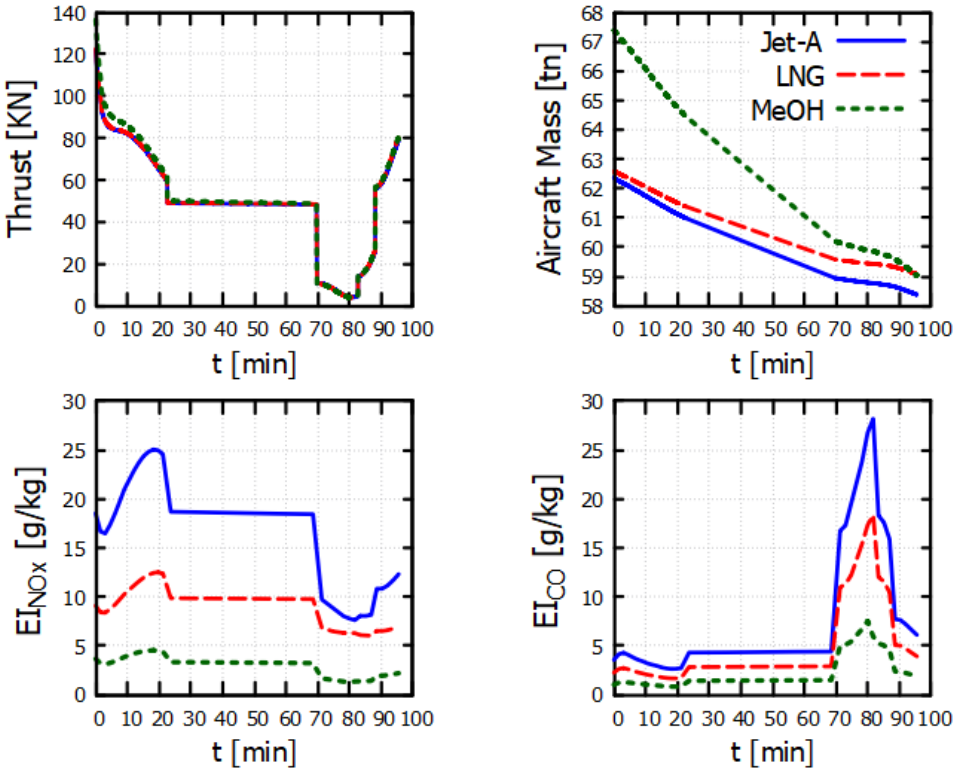

Figure 17. Thrust, aircraft total mass and EI time series for the London–Barcelona mission.

5. Discussion

The integration of a CANTERA-based component into the PROOSIS environment represents the primary novelty of this study, enabling aero-engine models to efficiently evaluate a wide range of fuels, provided a corresponding plug-in combustion mechanism is available. This approach eliminates the need to determine fuel-specific thermal properties (e.g., LHV) and combustion efficiency correlations, typically bare minimum requirements for evaluating alternative fuels on a 0-D level. Instead, if the base chemical composition of the fuel is known or approximated, the evaluation process becomes significantly streamlined. Previous studies using PROOSIS relied on correlation methods to predict emission trends and fuel efficiency variations [31,33]. In contrast, the proposed model introduces added generality for estimating aero-engine emissions and design-sensitive parameters related to the burner. This added capability is particularly valuable for engine and mission design analyses [43].

The evaluation of GTF operation fuelled by LNG and MeOH reasserts their literature-covered thrust-production ability within current engine setups coupled with their overall emission reduction potential. Furthermore, this study aims to facilitate the preliminary re-design of existing engines to optimally accommodate alternative fuels, both in terms of emissions and fuel consumption [30]. This is achieved by employing advanced, generalist burner models rather than the simplistic iterations commonly used in prior studies [20]. In practice, the GTF-adapted model was verified against corresponding ICAO data for Jet-A operation, demonstrating sufficient fidelity in predicting engine thermodynamic cycle and emissions, particularly for NO_x trends.

Considering the evaluation results of LNG and MeOH, focusing solely on the engine performance independent of its mission area of application, two approaches were adopted: one with a set-thrust equal to the baseline and the other with a set-TIT condition.

- Set-thrust evaluation of LNG and MeOH successfully addresses the current propulsive need of the A320neo and produces estimations which are in agreement with previous

studies. The results show that both fuels can store enough energy in the working medium to power the turbine and convert the rest into thrust while decreasing its post-combustion temperature and its overall emissions [10,19,20,24,25]. This further confirms that both fuels are potentially capable of powering an A320 aircraft with benefits for engine life and emissions, provided the modifications to the fuel supply and storage systems remain within the aircraft's weight and volume constraints. However, this mission evaluation approach should be further investigated to understand how these fuels are expected to reduce the operational range of the aircraft [1]. Moreover, the proven decrease in TIT when using such fuels suggests a possible reduction in the need for turbine cooling air bleeds. This opens up additional opportunities for optimization when considering an engine redesign with a set-F_N objective, as less cooling air bleed could improve overall engine efficiency and performance (through a snowball effect concerning the beneficial effect of bleed lowering to turbine efficiency reducing TIT even further).

- The set-TIT approach causes new insights to emerge regarding the impact of LNG and MeOH on the engine cycle and emission profiles. The previously discussed TIT-decrease margin can be forfeited to generate even greater thrust to accommodate the highlighted need of a greater TO thrust due to maximum TOW augmentation caused by either the cryogenic tank configuration for LNG [19] or by the absolute increase in $\dot{m}_f$ for MeOH [10,24]. This evaluation strategy achieves extra thrust by increasing fuel consumption, which in turn raises rotational speeds and enhances airflow and the OPR. The additional energy from the increased fuel use is distributed between the turbines and the exhaust jet momentum, both contributing to the thrust gain. However, this shift in operating conditions, moving away from the engine design point, should have a negative rather than a neutral impact on its lifespan. As a result, a redesign of the compressor block is advised to accommodate the higher thermal and energy demands when using LNG or MeOH under a set-TIT operating regime. Therefore, although the set-TIT operation offers a notable yet diminished overall emission reduction potential, it should not be regarded as a viable integration option for the fuels in question. Instead, it highlights the potential benefits of aero-engine redesign in the context of alternative fuels. Engine models such as the one proposed, coupled with multidisciplinary engine design methods, could be crucial for the development of fuel-specific engine re-sizing solutions or even novel configurations, as emphasized by the authors in [43].

Finally, for the aircraft mission analysis, the proposed engine model is integrated with an in-house flight evaluation tool. Assuming an A320 is retrofitted to run on LNG or MeOH, the analysis demonstrates that using these fuels for an average European mission range is feasible without exceeding the aircraft's weight restrictions. This is achievable because, although $\dot{m}_f$ shows a linear relationship with changes in total FW (a slight decrease for LNG and a twofold increase for MeOH), the maximum Take-Off Weight (TOW) remains largely unchanged for LNG and only slightly increases for MeOH. As a result, the net-thrust profile of the mission remains nearly identical for both fuels, confirming that the set-F_N operation is a valid assumption for evaluating alternative fuels, if assumed that no changes are made to the aircraft's aerodynamic design and that the mission range is within certain limits. Finally, regarding all evaluated emissions, again, both fuels display reduction capabilities, with LNG having an advantage in reducing CO_2 and CO, with MeOH showing greater potential for NO_x.

6. Conclusions

To conclude, a 0-D GTF model with an integrated detailed chemistry isobaric burner was developed, tested and applied to evaluate two non drop-in fuels, LNG and MeOH. A robust simulation framework combining the PROOSIS v6.2.0 software and a detailed CRN model was successfully coupled to assess the thermodynamic and emission performance of the fuels. The integration of advanced CRN techniques allowed for more detailed analysis of the combustion process, pollutant formation mechanisms and the impact of alternative fuel properties on engine performance. The proposed model provided a detailed and accurate analysis of LNG and MeOH as alternative aviation fuels while even being capable of producing cycle and emission predictions during a simulation of real flight scenario.

LNG stands out as a near-term solution with manageable integration efforts and enhanced emission mitigation and minor cycle improvement abilities in every evaluated scenario. Emission-wise, its LTO reduction potential compared to Jet-A, ranges from 19–21% for CO_2, 45–48% for NO_x and constant 39% for CO, depending on the thrust or TIT requirements assumed. Despite its challenges, MeOH demonstrates strong potential as a long-term alternative fuel, offering exceptional post-combustion temperature reduction and NO_x reduction capabilities, albeit with increased fuel storage requirements. Cycle-wise MeOH causes fuel mass consumption to increase by 105% while also reducing TIT by an average of 3% under set-F_N operation. Additionally, under set-TIT operation, MeOH holds the ability to increase thrust by 10%. Emission-wise, it is capable of reducing CO_2, NO_x and CO LTO emissions by 2–10%, 55–64% and 39%, respectively. Finally, both fuels are capable of carrying out an average European mission, representing a major area of application for the examined engine while also mitigating the overall emission footprint of the aircraft, in accordance with aforementioned numerical results. Yet no conclusions should be drawn regarding the current profitability of the evaluated alternative fuels in aviation.

Future research on alternative fuel integration in aviation should focus on expanding this work by integrating the proposed models within multidisciplinary preliminary engine design methods, enabling optimization with respect to performance, engine life and emissions. The focus should be on optimizing aero-engines by addressing the unique challenges associated with each fuel type while leveraging their respective advantages. This approach requires the integration of state-of-the-art 0-D engine models which incorporate detailed chemistry for combustor modeling, such as the one proposed. This would allow for more tailored solutions, enhancing the performance and efficiency of engines powered by alternative fuels.

Last but not least, to fully evaluate the viability of LNG and MeOH integration in the aviation industry, future research should include a more in-depth critical analysis of logistical and economic issues, such as fuel supply infrastructure, required aircraft and engine modifications and cost and risk assessment of these non-drop-in fuels. For example, the impact of LNG or methanol on mission range limits should be addressed in future work concerning this topic. Nevertheless, the computational tools developed in this work should serve as a valuable asset in undertaking such analyses. Demonstrating the advantages of these alternative fuels over the baseline performance of current engines is essential to justify the industry's investment in their costly integration.

Author Contributions: Conceptualization, K.M., S.V. and A.A.; methodology, S.V. and A.A.; software, S.V., N.A. and A.A.; validation, S.V.; formal analysis, S.V.; investigation, A.A. and S.V.; data curation, S.V.; writing—original draft preparation, S.V.; writing—review and editing, S.V., A.A. and K.M.; visualization, S.V.; supervision, A.A., N.A. and K.M.; project administration, N.A. and K.M.; funding acquisition, A.A., N.A. and K.M. All authors have read and agreed to the published version of the manuscript.

Funding: This research has been co-financed by the European Regional Development Fund of the European Union and Greek national funds through the Operational Program Competitiveness, Entrepreneurship, and Innovation under the call RESEARCH–CREATE–INNOVATE (project code: T2EDK-00034—Advanced alternative ground and air transport fuels fromresidual lipids—Lipid4fuel).

Data Availability Statement: The data contained within this article are available upon request from the corresponding author.

Conflicts of Interest: The authors declare no conflicts of interest.

Nomenclature and Symbols

The following abbreviations are used in this manuscript, while the symbols referred to in this paper are presented below :

a.k.a.	also known as
w.r.t.	with respect to
eq.	equation
Alt	Altitude
App	Approach
BADA	Base of Aircraft Data
BPR	By-pass Ratio
CAMACM	Commercial Aircraft Mission Analysis Computational Model
Cl	Climb
CRN	Chemical Reactor Network
DZ	Dilution Zone
FAR	Fuel to Air Ratio
FW	Fuel Weight
GHG	Green House Gas
GTF	Geared Turbofan
HC	Hydrocarbon
ICAO	International Civil Aviation Organization
Id	Idle
LHV	Lower Heating Value
LNG	Liquefied Natural Gas
LTO	Landing & Take-Off
LTT	Laboratory of Thermal Turbomachines
MeOH	Methanol
NTUA	National Technical University of Athens
OF	Objective Function
OPR	Overall Pressure Ratio
PROOSIS	PRopulsive Object-Oriented SImulation Software
PS	Power Setting
PZ	Primary Zone
RQL	Rich-Quench-Lean
SAF	Sustainable Aviation Fuel
SZ	Secondary Zone
TIT	Turbine Inlet Temperature
TO	Take-Off
TOW	Take-Off Weight
TSFC	Thrust Specific Fuel Consumption
UHC	Unburnt Hydrocarbons

Symbol	Description	Units
A_{ref}	Burner Reference Area	m^2
AR_i	Air Ratio per Zone$-i$	-
EI_k	Emission Index of species$-k$	g/kg of fuel
FAR	Fuel-to-Air Ratio	-
F_N	Net Thrust	N
L	Liner Length	m
LR_i	Length Ration per Zone$-i$	-
$\dot{m}_{core}$	Core Massflow	kg/s
$\dot{m}_f$	Fuel flow	kg/s
P_t	Total Pressure	bar
T_{ad}	Adiabatic Post-combustion Temperature	Kelvin
T_t	Total Temperature	Kelvin
t	Aircraft Mission time	min
ϕ	Equivalence Ratio	-
ω	Adaptation Weight	-

Appendix A. Fuel Combustion Mechanisms and Compositions

For the simulation of the Jet-A fuel, the detailed kerosene combustion mechanism of J. Luche [44] is employed, as in the initial work concerning the CRN model [30]. This mechanism consists of 91 species and 991 corresponding reactions, developed specifically for Jet-A combustion simulation, being validated over 0.5–10 atm pressure, 300–1800 K gas temperature and 0.5–2.0 equivalence ratio ranges, while also including nitrous oxides formation and reduction reactions. The parameter ranges clearly overlap the respective ranges covered within this work. Given that real jet fuel can consist of over 300 different hydrocarbons (HCs), their quality and quantity depending on season and oil-well location [40], they cannot be all accounted for in 0D–1D models. Consequently, it is common practice [40,45] to group these hydrocarbons into fractions based on HC families (e.g., paraffins) and represent each family with a single species (e.g., n-decane). This type of fuel surrogate is typically tailored to each specific mechanism. For the Luche mechanism, the fuel surrogate composition is outlined in Table A1, indicating that $n - C_{10}H_{22}$ represents the paraffins, $cy - C_9H_{18}$ the naphthenes and $ph - C_3H_7$ the aromatics [44].

For the alternative fuels, LNG and MeOH, the GRI 3.0 [46] is utilized, a mechanism optimized for conditions of 1000–2500 K, pressures of 10 Torr–10 atm, and equivalence ratios of 0.1–5 in premixed systems. This mechanism is mostly applied in natural gas combustion applications but also includes MeOH in its species pool. Typical LNG composition is assumed containing mostly methane, while the MeOH is assumed 100% pure, as seen in Table A1.

Table A1. Fuel parameters for the CRN model.

Parameter	**Jet-A**	**LNG**	**MeOH**
Mechanism	Luche [44]	GRI 3.0 [46]	
Composition (as molar ratios)	74% $n - C_{10}H_{22}$ 11% $cy - C_9H_{18}$ 15% $ph - C_3H_7$	90% CH_4 6% C_2H_6 4% C_3H_8	100% CH_3OH

Appendix B. PW1127G Performance Reference Data

Table A2. PW1127G reference ICAO data [37].

PW**1127**G	**Take-Off**	**Climb**	**Approach**	**Idle**
PS [%]	100	85	30	7
F_n [KN]	120.430	102.365	36.129	8.430
$\dot{m}_f$ [kg/s]	0.8	0.67	0.232	0.08
EI_{NOx} [g/kg]	20.814	16.954	10.593	5.203
EI_{CO} [g/kg]	0.268	0.362	4.885	24.526
EI_{UHC} [g/kg]	0.070	0.067	0.058	0.458
OPR [-]	31.7		-	
BPR [-]	12.3		-	

Appendix C. CRN Model: Adaptation of Geometric and Flow Input Data

Table A3. Adjusted parameters for the CRN burner model of the GTF.

Parameter	**Initial**	**Adapted**
A_{ref} [m^2]	0.126	0.126
L [m]	0.161	0.161
LR_{PZ} * [%]	29.90	34.05
LR_{SZ} [%]	33.60	33.60
LR_{DZ} [%]	36.50	32.35
ϕ_{PZ} * [-]	1.1	1.276
ϕ_{SZ} [-]	0.6	0.722

* active DVs during adaptation process.

Appendix D. A320 London–Barcelona Mission Data and Assumptions

The software used for the mission analysis of the engine model is CAMACM (Commercial Aircraft Mission Analysis Computational Model), a tool developed by LTT/NTUA [47]. The aircraft is simulated as a point mass upon which all forces act, such as lift, drag, thrust and weight. Environmental conditions are based on the International Standard Atmosphere [48], while air conditions are assumed stationary, homogeneous, ideal, and free of moisture.

The Airbus A320 aircraft is chosen for being an actual area of application for the PW1000. It is configured with 150 passengers and an additional 15% reserve fuel. Therefore, the payload corresponds to 14.25 tons, assuming that each passenger and their luggage have a combined mass of 95 kg. According to BADA v3.9 file [42], the A320 has the following specifications:

- Maximum TOW: 77 tons
- Maximum Payload: 21.5 tons
- Maximum FW: 20 tons
- Operating Empty Weight: 41.345 tons

Due to its cryogenic nature, LNG cannot be stored in the existing fuel tanks located in the wings. The A320 has four storage Compartments on the lower deck, shown in Figure A1, with compartments 1 and 5 easily accommodating the luggage needs of 150 passengers. Therefore, Compartments 3 and 4 can be used for LNG tanks, providing a total available volume of 18.1 m^3.

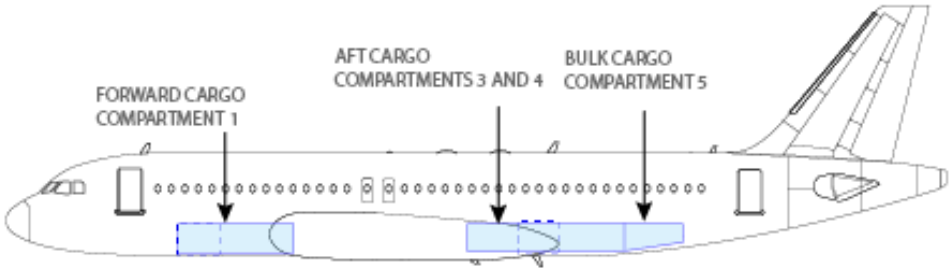

Figure A1. A320 cargo-hold compartments.

Due to the required characteristics of cryogenic fuel tanks (cylindrical with insulation) and the necessary space for piping and wiring, it is assumed that the usable fuel volume is 15 m^3. This means that 6960 kg of LNG can be stored in the tanks (with LNG density ρ_{LNG} = 464 kg/m^3). Considering the gravitational index (gravitational index = fuel mass/(fuel mass + tank mass)) for LNG is assumed to be 90% [19], the mass of the tanks is approximately 770 kg. Therefore, this additional mass is added to the OEW of the aircraft only when LNG is used to power the aircraft.

Finally, the mission flight route along with the aircraft's altitude and flight speed w.r.t. mission time are shown in Figure A2.

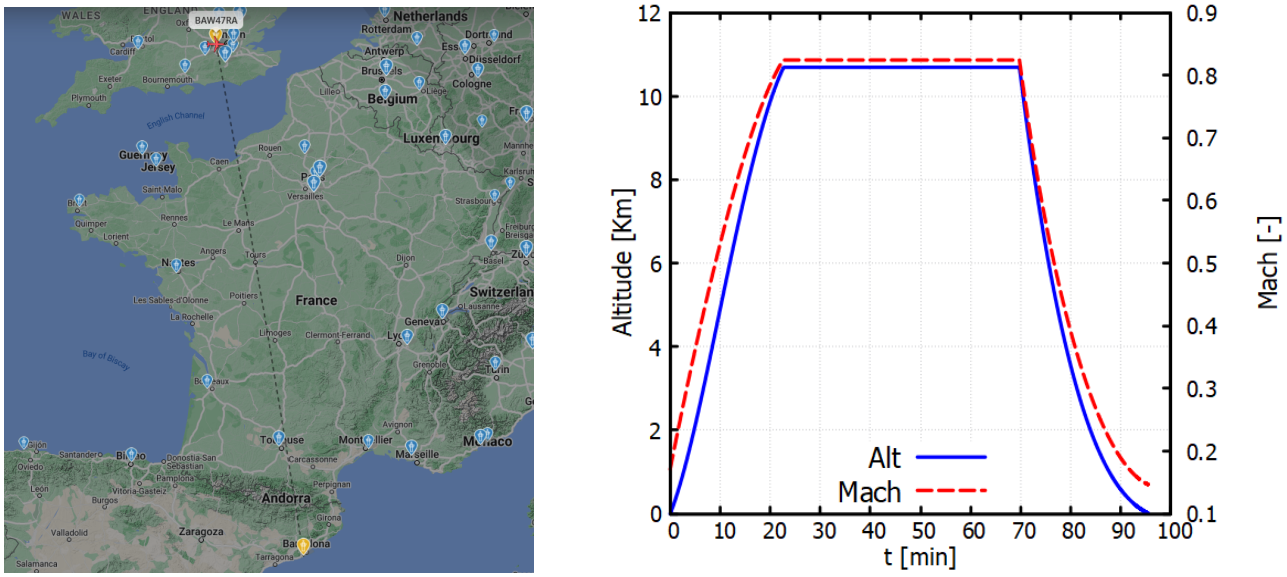

(**a**) (**b**)

Figure A2. Additional mission information. (**a**) Mission air-path over map [49]. (**b**) A320 altitude and speed time profiles, computed using CAMACM.

References

1. Ansell, P.J. Review of sustainable energy carriers for aviation: Benefits, challenges, and future viability. *Prog. Aerosp. Sci.* **2023**, *141*, 100919. [CrossRef]
2. Lai, Y.Y.; Christley, E.; Kulanovic, A.; Teng, C.C.; Björklund, A.; Nordensvärd, J.; Karakaya, E.; Urban, F. Analysing the opportunities and challenges for mitigating the climate impact of aviation: A narrative review. *Renew. Sustain. Energy Rev.* **2022**, *156*, 111972.
3. Marszałek, N.; Lis, T. The future of sustainable aviation fuels. *Combust. Engines* **2022**, *191*, 29–40. [CrossRef]
4. Grewe, V.; Rao, A.G.; Grönstedt, T.; Xisto, C.; Linke, F.; Melkert, J.; Middel, J.; Ohlenforst, B.; Blakey, S.; Christie, S.; et al. Evaluating the climate impact of aviation emission scenarios towards the Paris agreement including COVID-19 effects. *Nat. Commun.* **2021**, *12*, 3841. [CrossRef]

5. Lee, D.S.; Fahey, D.W.; Skowron, A.; Allen, M.R.; Burkhardt, U.; Chen, Q.; Doherty, S.J.; Freeman, S.; Forster, P.M.; Fuglestvedt, J.; et al. The contribution of global aviation to anthropogenic climate forcing for 2000 to 2018. *Atmos. Environ.* **2020**, *244*, 117834. [CrossRef]
6. Yin, F.; Rao, A.G. Climate impact of aviation emissions and the implications on aircraft engine design. In Proceedings of the Tutorial Handout of the ASME Turbo Expo 2022 Turbomachinery Technical Conference and Exposition GT2022, Rotterdam, The Netherlands, 13–17 June 2022; Volume 206.
7. Herzog, T. *World Greenhouse Gas Emissions in 2005*; WRI Working Paper; World Resources Institute: Washington, DC, USA, 2009.
8. International Energy Agency. Global Energy Review: CO_2 Emissions in 2021. 2022. Available online: https://www.iea.org/reports/global-energy-review-co2-emissions-in-2021-2 (accessed on 10 December 2024).
9. Christodoulakis, J.; Karinou, F.; Kelemen, M.; Kouremadas, G.; Fotaki, E.F.; Varotsos, C.A. Assessment of air pollution from Athens International Airport and suggestions for adaptation to new aviation emissions restrictions. *Atmos. Pollut. Res.***2022**, *13*, 101441. [CrossRef]
10. Price, R.O. Methanol: An Environmentally Attractive Alternative Commercial Aviation Fuel. In Proceedings of the IEEE 25th Intersociety Energy Conversion Engineering Conference, Reno, NV, USA, 12–17 August 1990; Volume 4, pp. 331–336.
11. Altarazi, Y.S.M.; Talib, A.R.A.; Yusaf, T.; Gires, J.Y.E.; Ghar, M.F.A.; Lucas, J. A review of engine performance and emissions using single and dual biodiesel fuels: Research paths, challenges, motivations and recommendations. *Fuel* **2022**, *326*, 125072. [CrossRef]
12. European Partnership. Clean Aviation: Strategic Research and Innovation Agenda. *EU Counc. Regul.* **2021**, *L 427*, 17–119.
13. Airbus. Cities, Airports & Aircraft. In *Global Market Forecast*; Airbus: Leiden, The Netherlands, 2019.
14. Liu, Z.; Deng, Z.; Davis, S.J.; Giron, C.; Ciais, P. Monitoring global carbon emissions in 2021. *Nat. Rev. Earth Environ.* **2022**, *3*, 217–219. [CrossRef]
15. Schripp, T.; Anderson, B.E.; Bauder, U.; Rauch, B.; Corbin, J.C.; Smallwood, G.J.; Lobo, P.; Crosbie, E.C.; Shook, M.A.; Miake-Lye, R.C.; et al. LeClercq. Aircraft engine particulate matter emissions from sustainable aviation fuels: Results from ground-based measurements during the NASA/DLR campaign ECLIF2/ND-MAX. *Fuel* **2022**, *325*, 124764. [CrossRef]
16. Sethi, V. *ENABLing CryogEnic Hydrogen Based CO_2 free Air Transport (ENABLEH2)*; Technical Report 8146886; Publications Office of the European Union: Luxembourg, 2022.
17. Przysowa, R.; Gawron, B.; Lecki, T.B.; Legowik, A.; Merkisz, J.; Jasinski, R. Performance and emissions of a microturbine and turbofan powered by alternative fuels. *Aerospace* **2021**, *8*, 25. [CrossRef]
18. Chiong, M.C.; Chong, C.T.; Ng, J.; Lam, S.S.; Tran, M.; Chong, W.W.F.; Jaafar, M.N.M.; Valera-Medina, A. Liquid biofuels production and emissions performance in gas turbines: A review. *Energy Convers. Manag.* **2018**, *173*, 640–658. [CrossRef]
19. Rompokos, P.; Kissoon, S.; Roumeliotis, I.; Nalianda, D.; Nikolaidis, T.; Rolt, A. Liquefied Natural Gas for Civil Aviation. *Energies* **2020**, *13*, 5925. [CrossRef]
20. Sasi, S.; Mourouzidis, C.; Roumeliotis, I.; Nikolaidis, T.; Pachidis, V.; Norman, J. Impacts of Alternative Aviation Fuels on Engine Cycle Design and Aircraft Mission Capability. In Proceedings of the ASME Turbo Expo 2023: Turbomachinery Technical Conference and Exposition. Volume 2: Ceramics and Ceramic Composites; Coal, Biomass, Hydrogen, and Alternative Fuels, Boston, MA, USA, 26–30 June 2023; ASME: New York, NY, USA, 2023; p. V002T03A005.
21. Seyam, S.; Dincer, I.; Agelin-Chaab, M. Novel hybrid aircraft propulsion systems using hydrogen, methane, methanol, ethanol and dimethyl ether as alternative fuels. *Energy Convers. Manag.* **2021**, *238*, 114172. [CrossRef]
22. Santasalo-Aarnio, A.; Nyari, J.; Wojcieszyk, M.; Kaario, O.; Kroyan, Y.; Magdeldin, M.; Larmi, M.; Järvinen, M. *Application of Synthetic Renewable Methanol to Power the Future Propulsion*; SAE Technical Paper 2020-01-2151; SAE: Warrendale, PA, USA, 2020.
23. Verhelst, S.; Turner, J.W.G.; Sileghem, L.; Vancoillie, J. Methanol as a fuel for internal combustion engines. *Prog. Energy Combust. Sci.* **2019**, *70*, 43–88. [CrossRef]
24. Dodds, W.J.; Ekstedt, E.E.; Bah, D.W. Methanol combustion in a CF6l-80A engine combustor. In Proceedings of the AIAA/SAE/ASME, 19th Joint Propulsion Conference, Seattle, WA, USA, 27–29 June 1983.
25. Cican, G.; Mirea, R.; Rimbu, G. Experimental Evaluation of Methanol/Jet-A Blends as Sustainable Aviation Fuels for Turbo-Engines: Performance and Environmental Impact Analysis. *Fire* **2024**, *7*, 155. [CrossRef]
26. Liu, Y.; Sun, X.; Sethi, V.; Li, Y.; Nalianda, D.; Abbott, D.; Gauthier, P.; Xiao, B.; Wang, L. Development and application of a preliminary design methodology for modern low emissions aero combustors. *Proc. Inst. Mech. Eng. Part A J. Power Energy* **2021**, *235*, 783–806. [CrossRef]
27. Nozari, M.; Eidiattarzade, M.; Tabejamaat, S.; Kankashvar, B. Emission and performance of a micro gas turbine combustor fueled with ammonia-natural gas. *Int. J. Engine Res.* **2022**, *23*, 1012–1026. [CrossRef]
28. Valles, M.A.; Kessler, I.; Windom, B.C. Review and Development of Natural Gas/Hydrogen Fuel Flexible Reduced Chemical Mechanism for High-Order Modeling of Gas Turbines. In Proceedings of the ASME Turbo Expo 2023: Turbomachinery Technical Conference and Exposition. Volume 3A: Combustion, Fuels, and Emissions, Boston, MA, USA, 26–30 June 2023; ASME: New York, NY, USA, 2023; p. V03AT04A030.

29. Vogel, M.; Kaufmann, J.; Völkl, V.; Hirsch, C.; Sattelmayer, T. Comparison of Equivalence Ratio Fluctuations in a Lean Premixed Combustor for Kerosene and Natural Gas. In Proceedings of the ASME Turbo Expo 2023: Turbomachinery Technical Conference and Exposition. Volume 3A: Combustion, Fuels, and Emissions, Boston, MA, USA, 26–30 June 2023; ASME: New York, NY, USA, 2023; p. V03AT04A011.
30. Villette, S.; Adam, D.; Alexiou, A.; Aretakis, N.; Mathioudakis, K. A Simplified Chemical Reactor Network Approach for Aeroengine Combustion Chamber Modeling and Preliminary Design. *Aerospace* **2024**, *11*, 22. [CrossRef]
31. Alexiou, A.; Aretakis, N.; Kolias, I.; Mathioudakis, K. Novel Aero-Engine Multi-Disciplinary Preliminary Design Optimization Framework Accounting for Dynamic System Operation and Aircraft Mission Performance. *Aerospace* **2021**, *8*, 49. [CrossRef]
32. Kurzke, J. Fundamental Differences Between Conventional and Geared Turbofans. In Proceedings of the ASME Turbo Expo 2009: Power for Land, Sea, and Air. Volume 1: Aircraft Engine; Ceramics; Coal, Biomass and Alternative Fuels; Controls, Diagnostics and Instrumentation; Education; Electric Power; Awards and Honors, Orlando, FL, USA, 8–12 June 2009; ASME: New York, NY, USA, 2023; pp. 145–153.
33. Alexiou, A. *Introduction to Gas Turbine Modelling with PROOSIS*, 4th ed.; Empresarios Agrupados International (EAI) S.A.: Madrid, Spain, 2020.
34. McKinney, R.; Cheung, A.; Sowa, W.; Sepulveda, D. The Pratt & Whitney TALON X Low Emissions Combustor: Revolutionary Results with Evolutionary Technology. In Proceedings of the 45th AIAA Aerospace Sciences Meeting and Exhibit, Reno, NV, USA, 1–8 January 2007.
35. Cantera Co. Cantera Is an Open-Source Suite of Tools for Problems Involving Chemical Kinetics, Thermodynamics, and Transport Processes. Available online: https://cantera.org (accessed on 10 December 2024).
36. Gordon, S.; McBride, B.J. *Computer Program for Calculation of Complex Chemical Equilibrium Composition and Applications*; NASA RP1311; NASA: Washington, DC, USA, 1994.
37. ICAO Aircraft Engine Emissions Databank. Available online: https://www.easa.europa.eu/en/domains/environment/icao-aircraft-engine-emissions-databank (accessed on 10 December 2024).
38. Lefebvre, A.H.; Ballal, D.R. *GAS Turbine Combustion: Alternative Fuels and Emissions*; CRC Press: Boca Raton, FL, USA, 2010.
39. Ranjith P. V, M. Shivashankar, G. Sivaramakrishna, Vimala Narayanan. Reduction of Gas Turbine Combustor Pattern Factors using CFD. *Int. J. Eng. Res. Technol.* **2014**, *3*, 1786–1791.
40. Braun-Unkhoff, M.; Riedel, U. Alternative fuels in aviation. *CEAS Aeronaut J.* **2015**, *6*, 83–93. [CrossRef]
41. EUROCONTROL Think Paper #21–22 August 2023. Available online: https://www.eurocontrol.int/sites/default/files/2023-08/eurocontrol-think-paper-21-long-haul-decarb.pdf (accessed on 10 December 2024).
42. Nuic, A. *User Manual for the Base of Aircraft Data (BADA)*, Revision 3.9; EUROCONTROL Experimental Centre Project BADA Report 11/03/08-08; Supporting European Aviation: Brussels, Belgium, 2011.
43. Alexiou, A.; Kolias, I.; Aretakis, N.; Mathioudakis, K. Aero-Engine Preliminary Design Optimization and Operability Studies Supported by a Compressor Mean-Line Design Module. *Aerospace* **2023**, *10*, 726. [CrossRef]
44. Luche, J. Obtention de Modeles Cinetiques Reduits de Combustion: Application a un Mecanisme du Kerosene. Ph.D. Thesis, Universite D'Orleans, Orléans, France, 2003.
45. Liu, J.; Zhang, D.; Hou, L.; Yang, J.; Xu, G. Laminar burning speed of aviation kerosene at low pressures. *Energies* **2022**, *15*, 2191; ISSN 1996-1073. [CrossRef]
46. Smith, G.P.; Golden, D.M.; Frenklach, M.; Moriarty, N.W.; Eiteneer, B.; Goldenberg, M.; Bowman, C.T.; Hanson, R.K.; Song, S.; Gardiner, W.C.; et al. GRI-Mech 3.0. 1999. Available online: http://www.me.berkeley.edu/gri_mech (accessed on 10 December 2024).
47. Kelaidis, M.; Aretakis, N.; Tsalavoutas, A.; Mathioudakis, K. Optimal Mission Analysis Accounting for Engine Aging and Emissions. *ASME J. Eng. Gas Turbines Power* **2009**, *131*, 011201. [CrossRef]
48. *ISO 2533:1975*; Standard Atmosphere; Edition 1. International Organization for Standardization: Geneva, Switzerland, 1975. Available online: https://www.iso.org/standard/7472.html (accessed on 10 December 2024).
49. Flight Radar 24. Available online: https://www.flightradar24.com (accessed on 10 December 2024).